WIND TURBINE DIFFUSER AERODYNAMIC STUDY WITH OPENFOAM

FELIX SORRIBES-PALMER, ANTONIO FIGUEROA, ANGEL SANZ ANDRES,

SANTIAGO PINDADO

Instituto de Microgravedad 'Ignacio Da Riva' Universidad Politécnica de Madrid (IDR/UPM),

felix.sorribes@upm.es

Keywords: *Wind Turbine, Diffuser, Openfoam, Aerodynamics*

Abstract

The aim of this work is to analyze the influence of the pressure losses of a diffuser augmented wind turbine (DAWT) in the extractable power. Multi-element diffuser geometries, generated with Salome and meshed with snappyHexMesh, are studied numerically with OpenFOAM to find a configuration of maximum area expansion (reducing flow detachment), for different pressure losses at the actuator disk. Different geometries are studied with $k-\varepsilon$ turbulence model. The influence of the vanes inside the diffuser has been also analyzed. The results of the present works show the importance of a careful design of the diffuser entrance.

1 Introduction

As it is well known, the extractable energy of a horizontal-axis turbine rotor of fixed size can be increased by installing it at the entrance of a diffuser. By recovering exhaust kinetic energy, the diffuser produces a greatly reduced pressure behind the turbine compared to the one behind a bare turbine. This effect increases the mass flow-rate through the DAWT, with at least as much pressure change as across a conventional turbine [Gilbert et al., 1978]. The overall effect is to increase the power produced for a given rotor diameter. The increase of mass flow-rate in the diffuser is influenced by four main factors [Shives and Crawford, 2012]:

- The diffuser area ratio A_{ex}/A_c.
- The flow separation downstream in the diffuser.
- The base pressure reduction at the diffuser exit caused by the obstruction flow.
- Viscous losses.

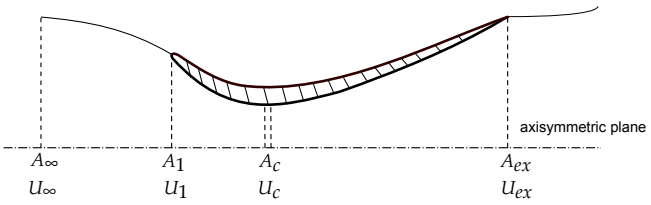

Figure 1.1: Sketch of a general DAWT duct. The areas and flow velocities at the characteristic section of the duct are indicated.

According to Blevins' Handboook [1984], the flow separation in a diffuser, also called diffuser stall, depends on: diffuser inlet and outlet conditions, Reynolds number, Mach number, and diffuser geometry. In this handbook, difusser stall is studied for different configurations two-dimensional, conical, annular, straight-walled and curved wall diffusers. Useful curves for different stall regimes (first appreciable, large transitory, fully developed, hysteresis zone and jet flow) for different difusser as a function of geometry parameters being included.

A general schema of a DAWT duct is shown in Figure 1.1. In this work a configuration with two slots in the diffuser is analyzed as an improvement, bearing in mind that the tangential injection of air available from the external wind supplied to the boundary layer helps the main flow overcome the adverse pressure gradient and frictional losses in the wall region.

Additionally, the effect of a vane installed in the duct was analyzed too. Vanes subdivide the diffuser into a series of diffusing passages, each of which will have divergence angles and area ratios much smaller than those of the vaneless diffuser [Blevins, 1984].

The present work is organized as follows: in Section 2, the main parameters of DAWT performance are presented. In Section 3, the CFD numerical setup of different configurations to find the maximum extractable power are presented. In Section 4 the results of the simulations are presented. Finally, in Section 5, the main conclusions of the numerical study are drawn.

2 Analytical Framework

The different cases are compared by analyzing the variation of pressure through the duct, from the energy conservation equation, for a steady and incompressible flow [Küchemann and Weber, 1953], the relation between the exit and freestream condition is given by:

$$p_\infty + \frac{1}{2}\rho U_\infty^2 = p_{ex} + \frac{1}{2}\rho U_{ex}^2 + \Delta p_c + \Delta p_d \,, \tag{2.1}$$

where Δp_c, Δp_d are the total pressure losses in the turbine and the duct, respectively. U_∞ and U_{ex} are the flow speed upstream and at the exit of the duct, respectively (see Figure 1.1). The total pressure losses can be modeled as:

$$\Delta p_c = k_{pc}\frac{1}{2}\rho U_c^2 \,, \quad \Delta p_d = k_{pd}\frac{1}{2}\rho U_c^2 \,. \tag{2.2}$$

Besides, the pressure loss coefficient in the turbine is:

$$K_{pc} = \frac{\Delta p_c}{\frac{1}{2}\rho U_c^2}\lambda^2 \,. \tag{2.3}$$

where $\lambda = U_c/U_{ex}$. From Betz's limit, it can be deduced that the pressure loss at a turbine related to extractable maximum energy is $K_{pc} \sim 2$ ([Lawn, 2003]).

The pressure coefficient at the diffuser exit is:

$$c_{pex} = \frac{p_{ex} - p_\infty}{\frac{1}{2}\rho U_\infty^2} \,, \tag{2.4}$$

where p_∞ and p_{ex} are respectively the static pressure of the flow upstream and at the exit.

Finally, the extracted power by the turbine can be estimated as:

$$c_{Wc} = \frac{\Delta p_c U_c A_c}{\frac{1}{2}\rho A_c U_\infty^3} = K_{pc}\lambda\left(\frac{U_{ex}}{U_\infty}\right)^3 \,. \tag{2.5}$$

This parameter is used in the present work to compare the different DAWT configurations.

3 Numerical setup

In order to simulate the different configurations, the open source CFD software OpenFOAM was used. To compare the performance of several DAWT duct configurations, a 2D model is proposed using a porous region as an actuator disk.

The length of the studied DAWT duct configurations is about 17 m, with a cross-section area ratio $\lambda = A_{ex}/A_c = 3.7$. The computational domain dimensions are 60mx24mx0.5m.The geometries were developed with Salome, by using a python script, which allowed to created parametric geometries. The meshes were generated with snappyHexMesh. The procedure followed was to generate the .stl files first. Then, the mesh was generated by employing surfaceFeatureExtract, snappyHexMesh and extrudeMesh.

In Figure 3.1 the duct geometry and two details of the mesh are shown. The final mesh is obtained from the castellation of the .stls geometries, as indicated in the aforementioned figure. Then the porosity region was assigned with topoSet using Darcy-Forchheimer formulation. Just inertial terms, F, were considered to take into account the effect of the porosity in this region. This term was included in the momentum equation as follows ([Hafsteinsson, 2009]):

$$\frac{\partial}{\partial t}(\rho u_i) + u_j\frac{\partial}{\partial x_j}(\rho u_i) = -\frac{\partial p}{\partial x_i} + \mu\frac{\partial \tau_{ij}}{\partial x_j} - \left(\mu D + \frac{1}{2}\rho u_{jj} F\right) u_i \,. \tag{3.1}$$

The porosity which simulates the turbine was localized at the narrow section of the duct along a length of 0.2 m. Each configuration has been simulated for several values of F.

The generated meshes provide y^+ about 12 in all studied cases. Although y^+ was smaller than 30, wall functions were used to model turbulence at the walls. The Reynolds number reached up to R_e ~550000 ($U_\infty = 4$ m/s) on

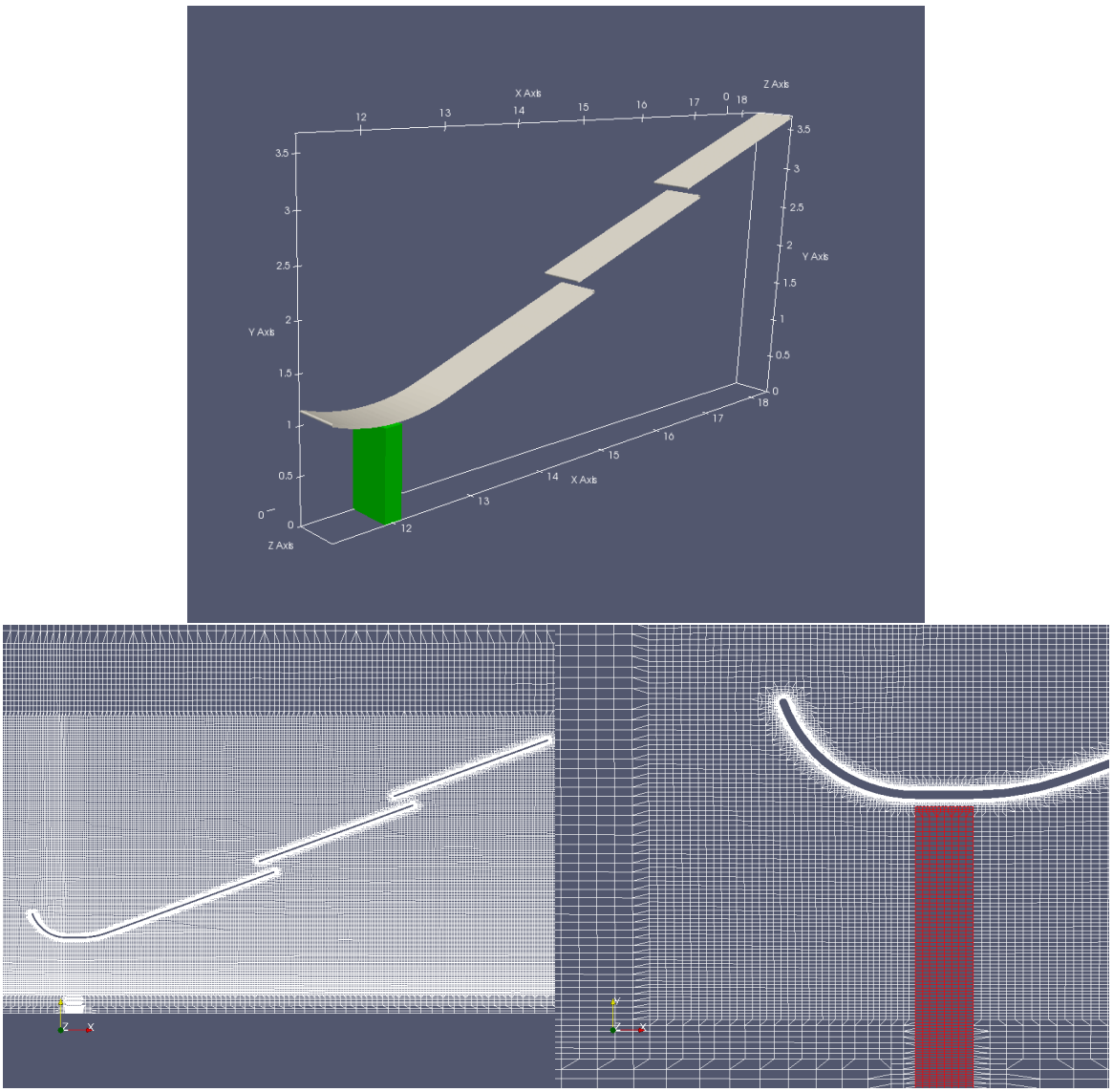

Figure 3.1: Top: geometry dimensions of the DAWT duct configurations. Bottom left: mesh around the duct. Bottom right: detail of the mesh close to the porous region.

the turbine section. The numerical simulation was performed on the steady RANS equations with $k-\varepsilon$ turbulence model. The turbulence intensity introduced at the inlet was $I_u = 0.04$, the turbulent kinetic energy being calculated as $k = \frac{3}{2}\left(I_u U_\infty\right)^{3/2}$, and the dissipation rate as $\varepsilon = \rho C_\mu k/\mu_t$, where $C_\mu = 0.09$ and $\mu_t = 1000 I\mu$.

The equations are numerically solved by means of the SIMPLE algorithm, least squares cell based solver was used. A bounded Gauss linear upwind difference scheme was used for spatial discretization. The used solver was porousSimpleFoam with moderate under-relaxation factors.

A velocity boundary was used at the inlet and a static pressure boundary was used at the outlet. The top wall was defined as no-slip boundary, and back and front as empty to simulate 2D domain. In addition, a symmetry plane boundary condition simulating the other half of the turbine is used. The residuals were monitored using PyFoamPlotRunner, being the convergence criteria to keep the residual values under 10^{-4}. The DAWT duct configurations analyzed are shown in Figure 3.2. The red zone represents the porous region simulating the turbine. From configuration 1a) to 1b) a interior vane was introduced to reduce detachment on the diffuser; from 1a) to 2a) the inlet was modified to avoid detachment at the leading edge of the diffuser; finally between 2a) and 2b) the aforementioned vane has was introduced again.

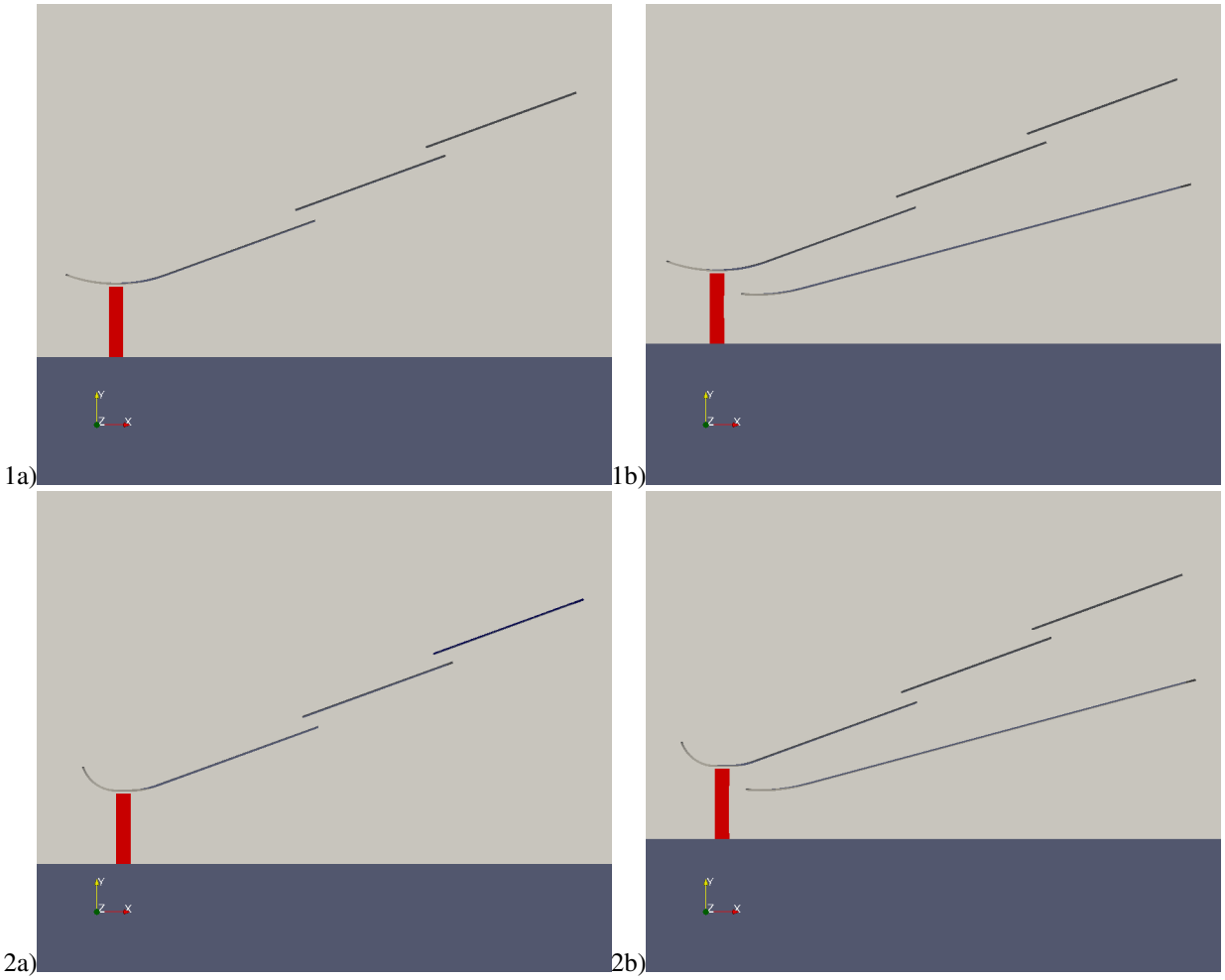

Figure 3.2: Diffuser augmented wind turbine configurations.

4 Results

Flow and pressure fields distribution are shown in Figures 4.1 and 4.2 for the different configurations analyzed. In Figure 4.2 can be appreciated how the vanes help to redistribute the pressure drop region.

The profiles of velocity and pressure at the different sections of the DAWT duct configurations are shown in Figure 4.3. These graphs indicate that the velocity profile at the first section of the duct is smoother in the configurations with the modified entrance. It can be also appreciated the flow acceleration in the gap between the porosity region and the diffuser, this helps to maintain the boundary layer attached. At the exit of the ducts, the velocity profile highlight the detached region. While adding a vane barely affects the pressure coefficient at the exit of the DAWT, it is significant that this coefficient decreases when the entrance of the diffuser is modified.

Comparing configurations 1a) and 1b), the effect of the vane is a reduction of the energy extracted. However, once the entrance was improved (configurations 2a) and 2b)), the vane implies an increase of the energy extracted.

The curves of extracted power coefficient and pressure coefficient are shown in Figure 4.4. The pressure coefficient has been estimated as an average of the pressure coefficient profile at the exit of the diffuser.

In Table 1 values of the maximum efficiency in relation to the different DAWT analyzed are summarized. Although the splitter vane helps to reattach the boundary layer at the difusser, as the flow detaches from the vane the pressure losses

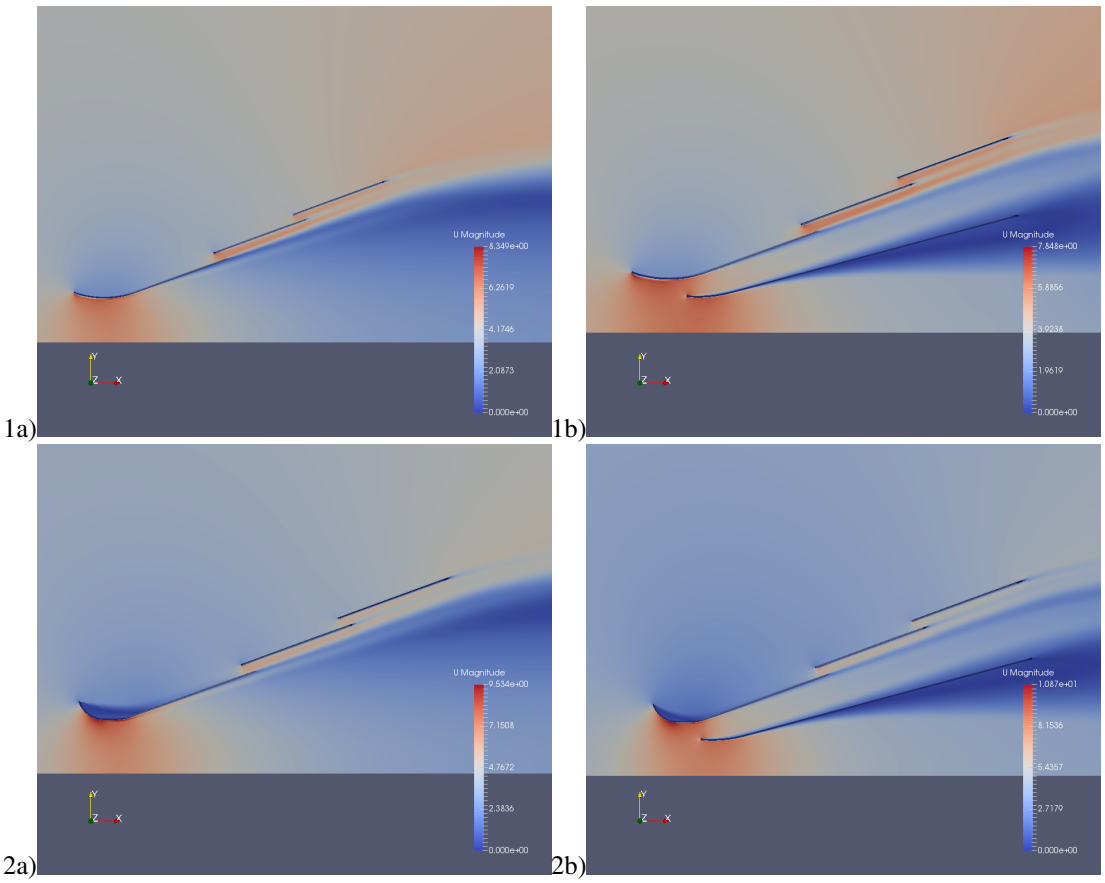

Figure 4.1: Velocity fields at the different DAWT configurations for the optimum K_{pc} for each configuration.

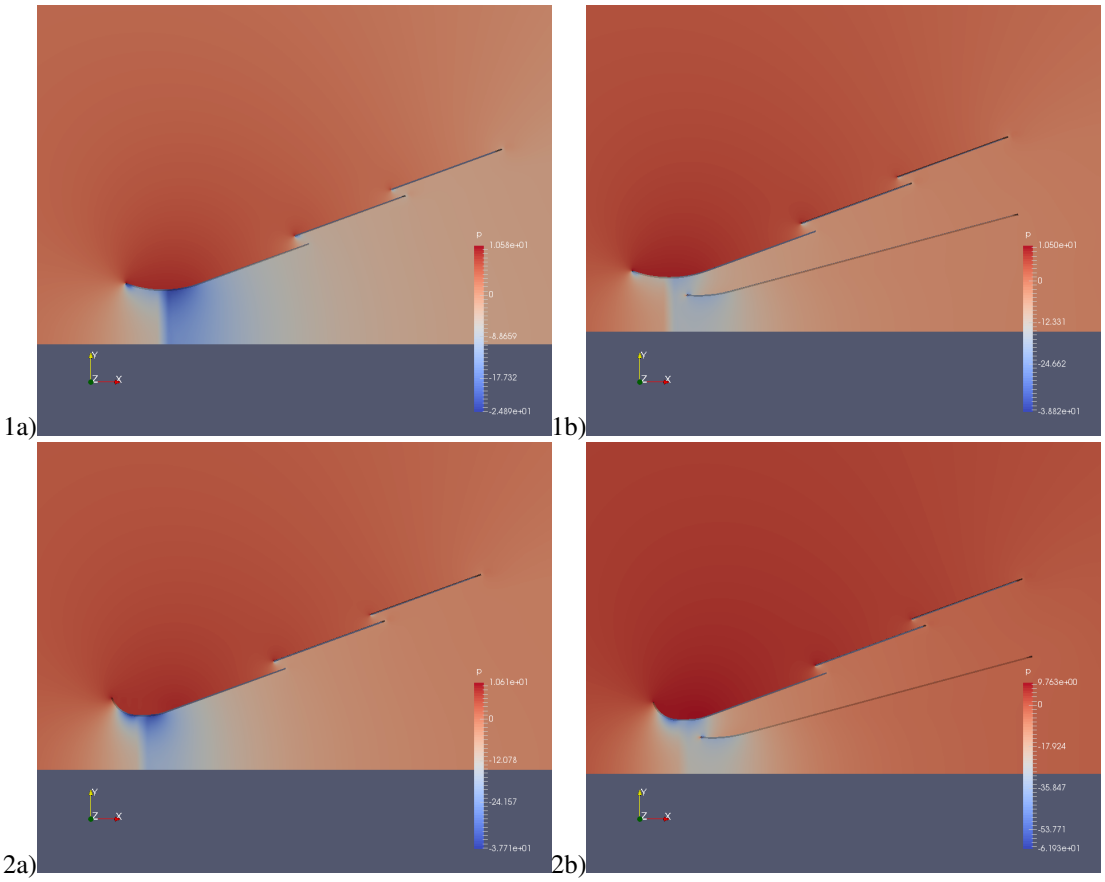

Figure 4.2: Pressure fields at the different DAWT configurations for the optimum K_{pc} for each configuration.

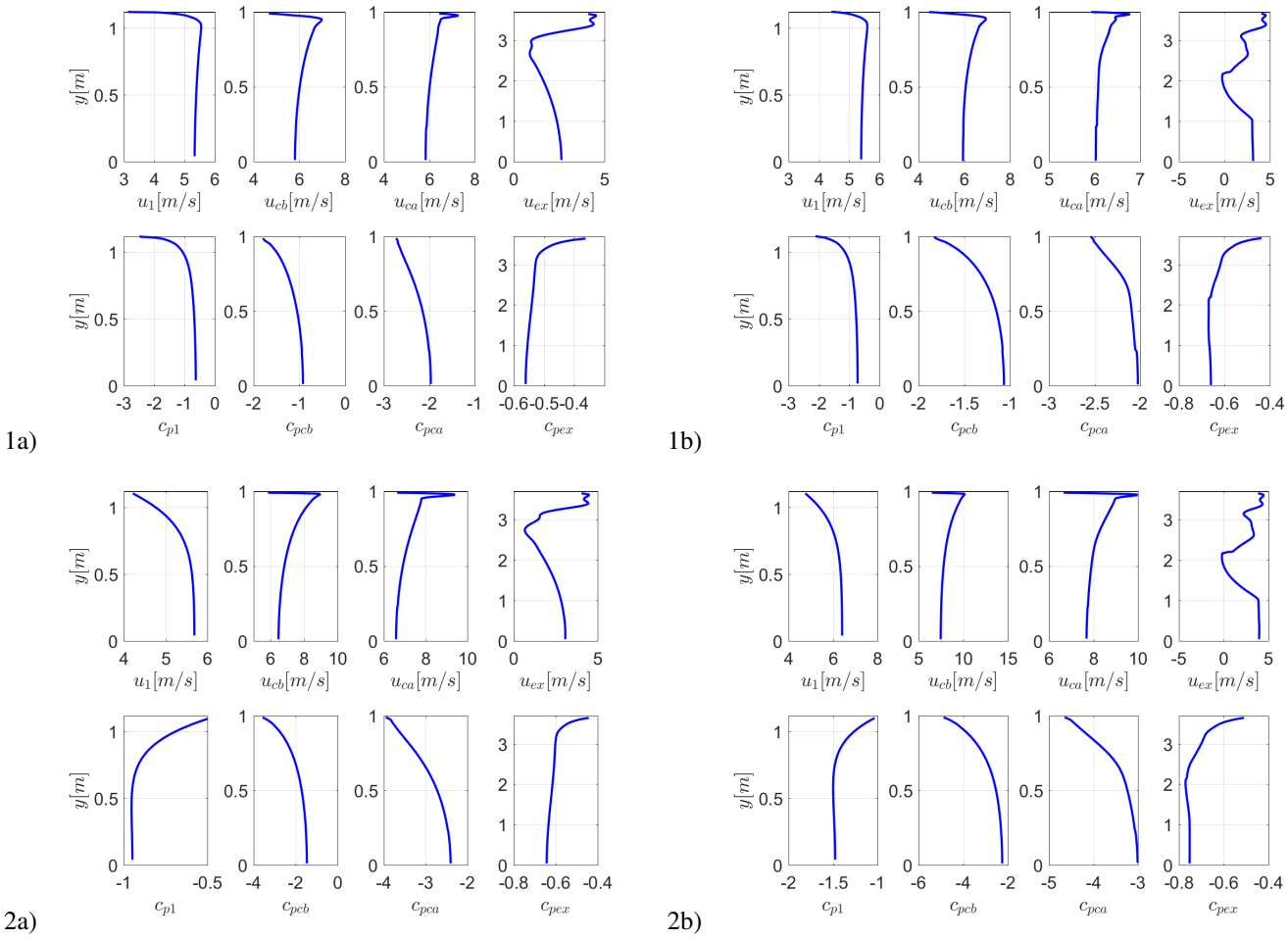

Figure 4.3: Velocity and pressure coefficient profiles in the sections A_1, A_{cb}, A_{ca} and A_{ex} for the optimum K_{pc} for each configuration.

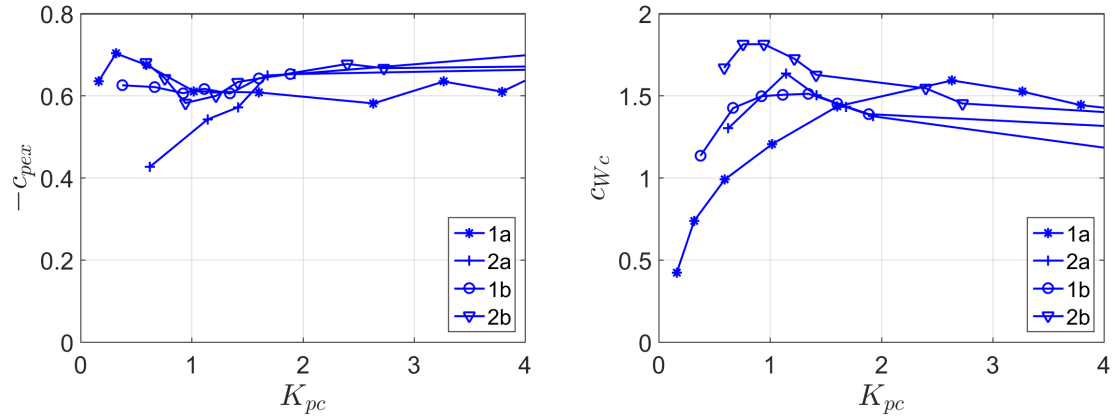

Figure 4.4: Pressure coefficient at the turbine exit and specific power extracted.

does not compensate because the configurations with vane do not improve the performance in all the simulated range of K_{pc}. A possible solution to this effect could be to split the vane or make it shorter to avoid flow detachment.

Table 1: Pressure loss coefficient K_{pc} at the for maximum extracted power coefficient C_{Wcmax} for the diffuser configurations.

Config.	Nº airfoils	K_{pcmax}	C_{Wcmax}
1a	3	1.76	1.6
1b	4	1.34	1.51
2a	3	1.14	1.63
2b	4	0.6	1.7

5 Conclusions

Four different configurations of DAWT ducts have been compared by obtaining the point of maximum extracted energy. The simulations show the importance of a well design entrance to the duct, in order to reduce pressure losses due to flow detachment. In addition, when the efficiency entrance increases, the optimum value of the extractable power was obtained for lower values of the coefficient K_{pc}, this result agrees with the work of Lawn [2003]. In comparison with configuration 1a), the flow is detached in 1b) in a part of the vane causing a reduction of the extractable power. However, when the entrance of the duct is enhanced, installing a vane increases the extractable energy. Accordingly, the configuration 2b) has the best performance. The obtained value of c_{Wc} exceeds the Betz limit for all configurations.

Acknowledgments

The authors thank all those involved in the organization of OFW11 and to all the contributors that will enrich this event OpenCFD [Apr. 2007]. We also want to thank OpenFoamWiki, CFDsupport, Chalmers University, ICE Stroemungsforschung for their contribution to OpenFoam documentation.

References

Robert D. Blevins. *Applied Fluid Dynamics Handbook*. New York, 1984. ISBN 9780442212964.

B.L. Gilbert, R.a. Oman, and K.M. Foreman. Fluid dynamics of diffuser-augmented wind turbines. *Journal of Energy*, 2 (6):368–374, 1978. ISSN 0146-0412. doi: 10.2514/3.47988.

Haukur Elvar Hafsteinsson. Porous Media in OpenFOAM. *Chalmers University of Technology. Thecnical Report*, 2009.

Dietrich Küchemann and Johanna Weber. *Aerodynamics of Propulsion*. McGraw-Hill, 1953.

C J Lawn. Optimization of the power output from ducted. In *Proceedings of the Institution of Mechanical Engineers–Part A– Power & Energy*, volume 217, pages 107–118, 2003.

OpenCFD. *OpenFOAM: The Open Source CFD Toolbox. User Guide Version 1.4, OpenCFD Limited*. Reading UK, Apr. 2007.

M. Shives and C. Crawford. Developing an empirical model for ducted tidal turbine performance using numerical simulation results. *Proceedings of the Institution of Mechanical Engineers, Part A: Journal of Power and Energy*, 226(1):112–125, 2012. ISSN 0957-6509. doi: 10.1177/0957650911417958.